UCONN LIBRARY

University of Connecticut
OpenCommons@UConn

Master's Theses | University of Connecticut Graduate School

8-23-2011

Development of Analytic Tools for Computational Flame Diagnostics

Mehrnaz Rouhi Youssefi
mehrnazrouhi@gmail.com

Recommended Citation
Rouhi Youssefi, Mehrnaz, "Development of Analytic Tools for Computational Flame Diagnostics" (2011). *Master's Theses*. 145.
https://opencommons.uconn.edu/gs_theses/145

This work is brought to you for free and open access by the University of Connecticut Graduate School at OpenCommons@UConn. It has been accepted for inclusion in Master's Theses by an authorized administrator of OpenCommons@UConn. For more information, please contact opencommons@uconn.edu.

Development of Analytic Tools for Computational Flame Diagnostics

Mehrnaz Rouhi Youssefi

B.S., University of Tehran, 2008

A Thesis

Submitted in Partial Fulfillment of the

Requirements for the Degree of

Master of Science

at the

University of Connecticut

2011

APPROVAL PAGE

Master of Science Thesis

Development of Analytic Tools for Computational Flame Diagnostics

Presented by

Mehrnaz Rouhi Youssefi, B.S.

Major Advisor _____

Tianfeng Lu

Associate Advisor _____

Chih-Jen Sung

Associate Advisor _____

Michael Renfro

University of Connecticut

2011

Acknowledgements

I am heartily thankful to my advisor, Dr. Tianfeng Lu, whose encouragement, guidance and support from the initial to the final level enabled me to develop an understanding of the subject.

I would like to also Thank Dr. Chih-Jen Sung, and Dr. Michael Renfro; my advisory committee.

Lastly, I offer my regards and blessings to all my family, friends, and colleagues who have supported me in any respect during the completion of this project.

Contents:

List of Figures

Chapter1. Introduction

Numerical simulation is an important approach in the research of chemically reacting flows, which may involve both turbulence and complex chemical reactions. Detailed chemical kinetics is frequently used in today's flame simulations due to its high fidelity in the chemical description. However, detailed chemical kinetics is typically complex and consists of a large number of species and reactions, such that it is frequently challenging to perform numerical simulations with detailed chemistry, and to analyze the simulation results. Analytic tools are important for computational flame diagnostics for the analysis of complex chemically reacting flows when detailed chemical kinetics is involved, due to the multi-timescale nature of detailed chemical kinetics, which renders simple numerical tools insufficiently accurate and consequently inapplicable. Analytic tools for detailed chemical kinetics research are based on analytically derived formula such that the accuracy in the computation results can be maximally retained. Such analytic tools are required in many cases to accurately compute flame properties and to enhance our understanding of various aspects of the combustion processes. For instance, a specific task in this work involves the determination of flame front locations, and limit phenomena such as ignition and extinction, in lifted jet flames using the chemical explosive mode analysis (CEMA) [1] based on the chemical Jacobian analytically derived for reduced mechanisms.

CEMA is a method based on eigenvalue analysis of the chemical Jacobian, and is more advantageous compared with the conventional diagnostics to detect critical flame characteristics based on temperature or an individual species concentration, which frequently require empirical or arbitrary selection of threshold values or isolines [1]. Eigenanalysis is

one of the most important tools to decouple complex couplings in reacting flows. Two prominent examples in combustion research involving eigenanalysis are the methods of intrinsic low-dimensional manifold (ILDM) [2] and the computational singular perturbation (CSP) [3-4]. CSP is a numerical method established in the mid 1980s [3-6], and has been primarily used in the analysis and reduction of stiff nonlinear ordinary differential equations (ODEs), particularly those involving detailed chemical kinetics. CSP has been applied for a variety of purposes in mechanism reduction, including the identification of quasi-steady state (QSS) species [7-10], elimination of unimportant species and reactions[11] and stiffness removal [12-14]. It has also been applied to analyze complex laminar flow–chemistry interactions[15], biochemical systems[16], counterflow ignition[17] and the auto-ignition in flow reactors [18]. CSP is based on a systematic separation procedure to separate the exhausted fast processes, which may be described with a set of algebraic equations rather than ODEs, from the slow processes. Hence fast and slow subspaces are decoupled. It was shown that the solutions with arbitrarily high order accuracy can be obtained with the CSP refinement procedure for nonlinear stiff ODEs [4, 19-21]. In many practical cases, the Jacobian matrix of the system of ODEs can be approximated as locally time-independent, particularly if only the time scales of the modes or species involved are of interest. In such cases, the time consuming CSP refinement procedure can be replaced by performing a simple eigen-decomposition of the Jacobian matrix [2, 9]. The concepts from CSP such as the radical pointer and the participation index [4], which indicates the contributions of species and reactions, respectively, can be utilized for mechanism reduction and computational flame diagnostics. In particular, the radical pointer can be employed to identify the candidate species to be solved by the algebraic equations. It has also been utilized in the

identification of QSS species and the fast species induced by partial equilibrium reactions [7-9, 22]. Many concepts in CSP were also extended in CEMA to quantify the contributions of species and reactions to the explosive chemical processes in combustion systems.

CEMA has been applied in many elementary combustion systems, including auto-ignition and premixed flames, as well as a turbulent lifted hydrogen jet flame into heated coflowing air computed by direct numerical simulation (DNS)[23-24]. In particular, auto-igniting mixtures and the locations of the lean premixed flame fronts were systematically identified using CEMA. Furthermore, CEMA clearly revealed that auto-ignition was the dominant stabilization mechanism in the turbulent lifted hydrogen jet flame in heated coflowing air, whereas it was shown not to be straightforward by using conventional methods based on individual scalars, such as temperature and a species concentration, to identify the stabilization mechanism of the lifted flame [23]. The previous CEMA work in [23-24]was based on the analytically derived Jacobian for skeletal mechanisms. In the present work, the analytic Jacobian for reduced mechanisms involving QSS species was further derived, such that CEMA can be performed directly with the reduced mechanisms employed in the DNS. As an extension to CEMA, explosive mode analysis (EMA) [24] that involve both the mixing processes and the chemical processes was developed. EMA will be discussed for a homogenous system of perfectly stirred reactors (PSR). Effort has also been made in the present work to extend EMA from homogeneous systems to diffusive flames, represented by the counterflow flames simulated with OPPDIF[25].

Chapter 2. Comparison of Analytical and Numerical Jacobians

Jacobian analysis is an important diagnostic approach for flames involving detailed chemistry. The Jacobian matrices in many numerical simulations, e.g. those in the CHEMKIN applications [26], were evaluated through numerical perturbation of the variables and re-evaluation of the functions involved. Such numerical perturbation approach often induces significant errors in the Jacobian that render the numerically evaluated Jacobian unreliable in computing the small eigenvalues, which is particularly important for CEMA because the chemical explosive modes are typically much slower than the fast modes induced by the fast reacting radicals. To resolve this problem, analytic Jacobian is required in CEMA as discussed in [1]. Analytic Jacobian for detailed chemistry was obtained by analytically differentiation of each reaction rates, including those with pressure fall-off and third bodies, with respect to temperature and species concentrations. Such analytic differentiation ensures that the maximal number of significant digits is retained in the Jacobian. To demonstrate the need for analytic Jacobian, Figure 1 shows the normalized errors in each entry of a numerical Jacobians for a stoichiometric hydrogen-air mixture in PSR at atmospheric pressure, inlet temperature of 900 K, and residence time of 1.1×10^{-4}s. The hydrogen mechanism which was used is a modification from Dryer's mechanism [27] by Ramanan Sankaran. Each cell in Fig. 1 indicates an entry in the Jacobian, and the normalized error, β, was defined as:

$$\beta = \frac{15 - \alpha}{15} \tag{2.1}$$

where α is defined as:

$$\alpha = -\log_{10}\frac{|J_N - J_A|}{|\max(J_N, J_A)|} \tag{2.2}$$

J_N and J_A are the numerical and analytical Jacobian matrices, respectively. In Figure 1 the first row is associated with energy equation and the 2nd to 10th row are associated with species equations of $H_2, O_2, O, OH, H_2O, H, HO_2, H_2O_2$, and N_2, respectively . The 1st to 9th column in Figure 1 are associated with the changes with respect to variations in species concentration in the aforementioned order, and the 10th column is associated with the changes with respect to temperature. It is noted that the 10th row in Fig. 1 which is associated with Nitrogen, which is not sensitive to perturbations, and hence, has the smallest errors represented by the white colors. On the other hand, column 10 which belongs to the derivatives of governing equations with respect to temperature which induces the largest errors as illustrated by darker colors. The dark gray cells in Fig. 1 indicates significant errors in the numerical Jacobian. While such errors will not result in significant errors in solving equations with Newton solvers, they are typically too large for CEMA. Therefore analytic Jacobian should be used to obtain reliable results for CEMA.

In addition to the high accuracy, analytical Jacobian is also efficient to evaluate as discussed in [28]. This is because the time spent on evaluating analytic Jacobian is linearly proportional to the number of reactions or species, while that for numerical Jacobian is a quadratic function of the number of reactions or species [28]. To demonstrate the higher efficiency of the analytical Jacobian, Figures 2 and 3 illustrate the computation time using analytic Jacobian in comparison with that with numerical Jacobian for hydrogen-air auto-ignition at different pressures and equivalence ratios. It is

seen that the CPU time and number of Jacobian evaluations were both reduced significantly using analytical Jacobian. Similarly, computation time for solving the PSR equations, and individual Jacobian matrix evaluation for different mechanisms using numerical and analytical Jacobian were shown for in Figs. 4-5, respectively. It is seen from Fig. 5 that the time saving by using the analytic Jacobian increases for larger mechanisms. The accuracy and efficiency of analytic Jacobian is therefore demonstrated. In the following, analytic Jacobian will be employed for diagnostics of detailed chemical kinetics in various flame applications.

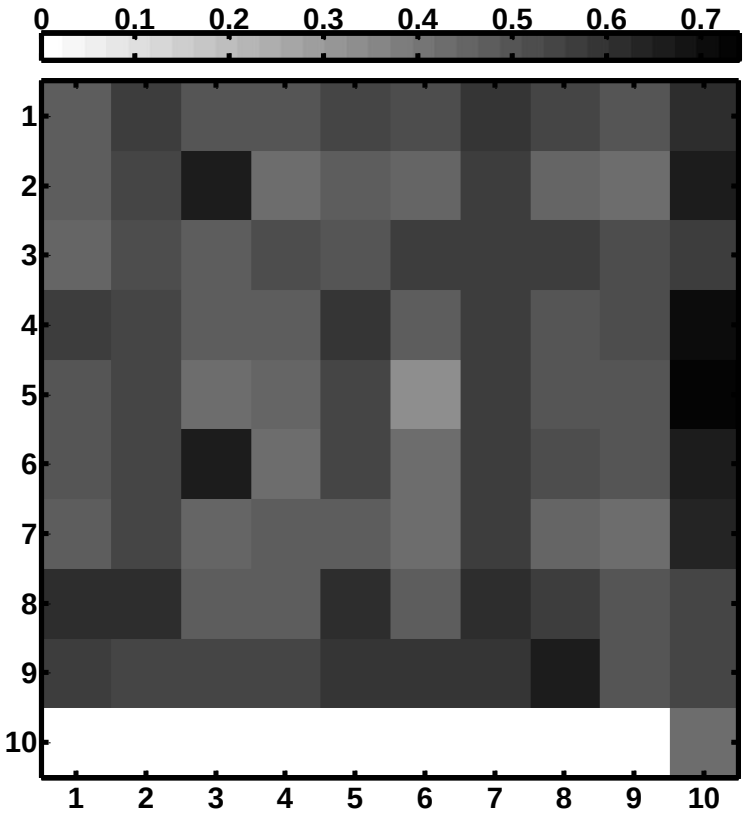

Figure 1. The normalized error of numerically evaluated Jacobian for the PSR solution of a stoichiometric hydrogen-air mixture at atmospheric pressure, inlet temperature of 900 K, and a residence time of 1.1×10^{-4} s. Dark colors indicate larger errors.

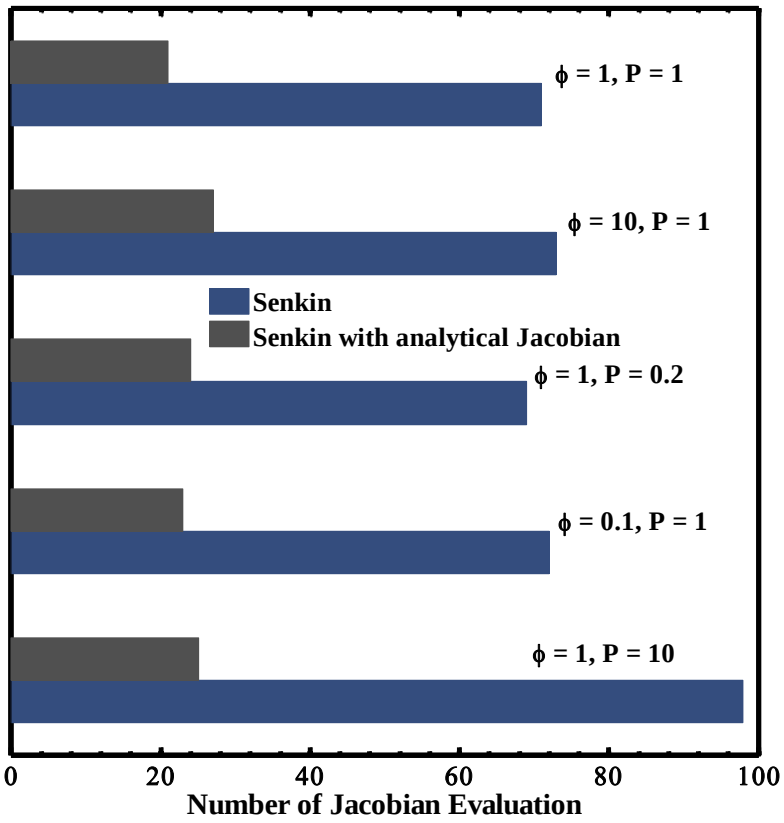

Figure 2. Comparison between the number of Jacobian evaluations using numerical and analytical Jacobian in Senkin for hydrogen auto-ignition with an inlet temperature of 900 K.

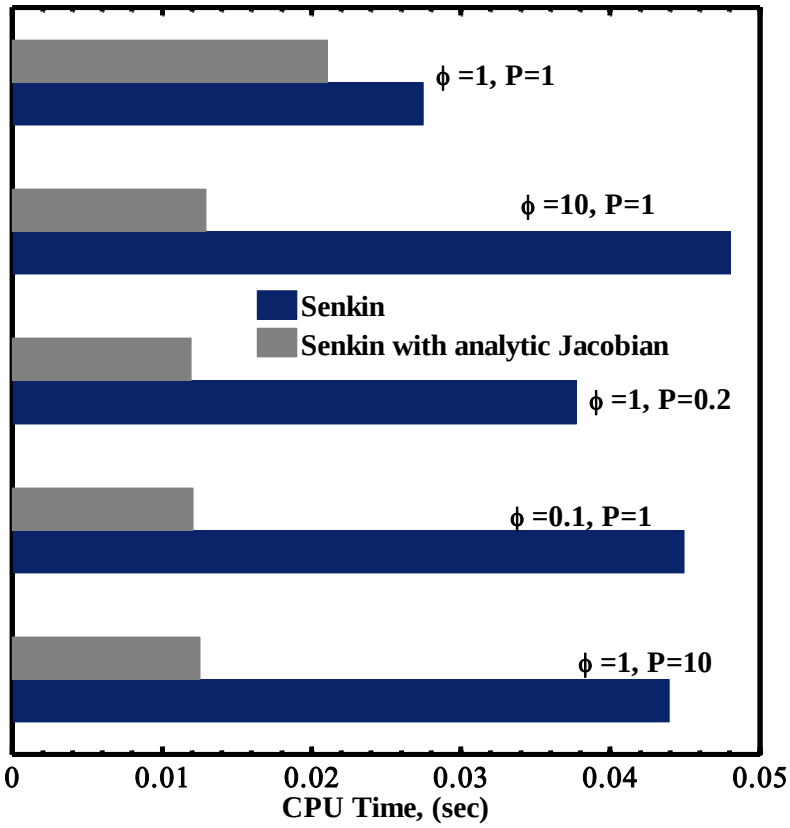

Figure 3.Comparison between required CPU time using numerical and analytical Jacobian in Senkin for autoignition of hydrogen-air mixtures with different equivalence ratios and an inlet temperature of 900 K.

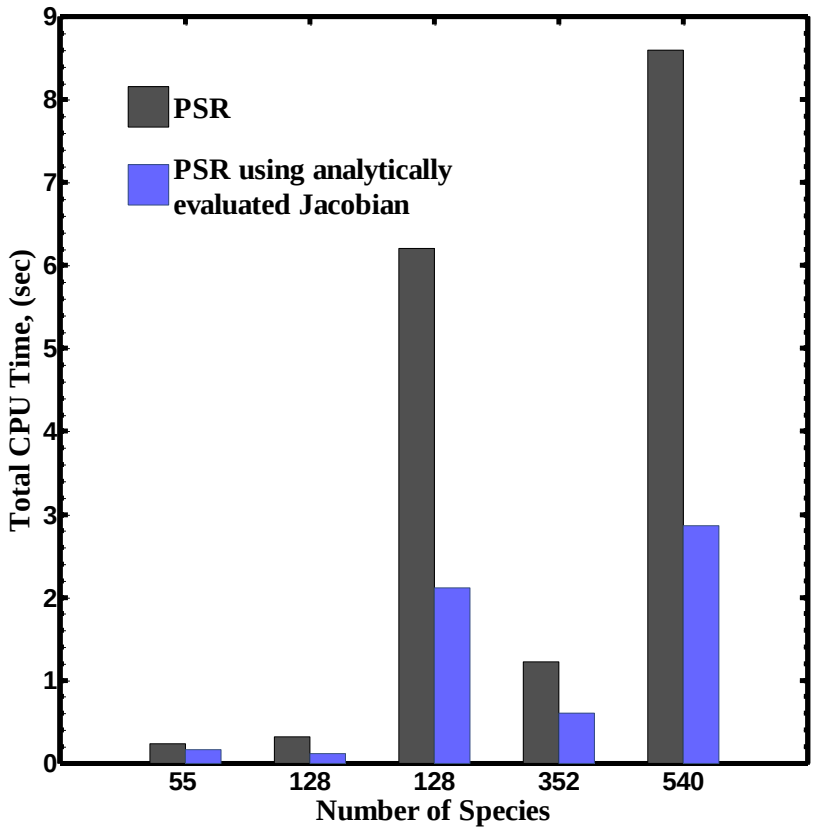

Figure 4. Comparison between the total CPU time using numerical and analytical Jacobian in PSR for different stoichiometric mixtures under atmospheric pressure and an inlet temperature of 900 K.

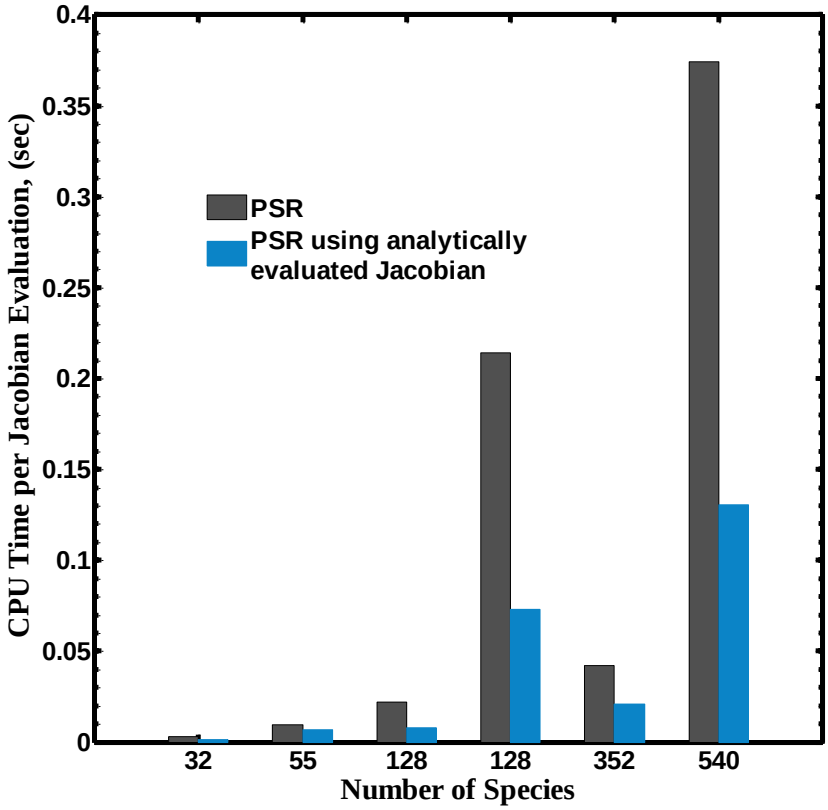

Figure 5. Comparison between the required CPU time per Jacobian evaluation using numerical and analytical Jacobian in PSR for different stoichiometric mixtures under atmospheric pressure and an inlet temperature of 900 K.

Chapter 3. Chemical Explosive Mode Analysis (CEMA) for Flame Diagnostics with Reduced Chemistry

3.1. Methodology of CEMA

CEMA is a systematic method for computational flame diagnostics involving detailed chemical kinetics [1]. As a brief review of CEMA, a general chemically reacting system can be formulated as the following ODE:

$$\frac{D\mathbf{y}}{Dt} = \mathrm{g}(\mathbf{y}) = \boldsymbol{\omega}(\mathbf{y}) + \mathbf{s}(\mathbf{y}) \qquad \textbf{(3.1.1)}$$

where D/Dt is the material derivative, **y** is the vector of dependent variables, such as species concentrations and temperature, **g** is the total source term which consists of the chemical source term **ω**, and all the non-chemical sources **s**, such as diffusion and homogeneous mixing. It's worth mentioning that for high dimensional flows, temperature and species concentrations at different locations correspond to different entries in **y**. Moreover, the convective term is included in the material derivative in eq. (3.1.1). The material derivative in eq. (3.1.1) can be replaced by d/dt in the Lagrangian coordinate system. The chemical Jacobian is defined as:

$$\mathbf{J}_{\boldsymbol{\omega}} = \frac{\partial \boldsymbol{\omega}}{\partial \mathbf{y}}, \qquad \textbf{(3.1.2)}$$

A chemical mode is an eigenmode associated with the chemical Jacobian. Furthermore, if the eigenvalue associated with a chemical mode has a positive real part, the chemical mode is a chemical explosive mode [1]. It is seen that if there is no mixing or loss

processes, i.e. **s** = 0, the chemical explosive mode will eventually lead to ignition. When the mixing or loss term is present, the chemical explosive mode may be strained by the loss or mixing, such that the system may not explode. Nevertheless, the presence of a CEM indicates the mixture's propensity to explode.

The chemical explosive modes are functions of temperature, mixture composition, and chemical reactivity. Therefore they can be considered as a chemical property of the mixture. These chemical properties of the mixture have been utilized for detection of ignition and extinction point, as well as flow classification in the upcoming sections [1, 23].

3.2. Sample Applications of CEMA: auto-ignition and lifted flames

It was shown in previous work that the existence of chemical explosive modes indicates the mixture's propensity to auto ignite if no loss is present [24, 29]. However, the temperature dependency of species enthalpy has not been considered in the evaluation of Jacobian matrix. Such a property can be used to detect both ignition and extinction in combustion systems. To demonstrate this point, Figure 6 shows the temperature profile and the reciprocal time scale of the chemical explosive mode in auto-ignition under constant pressure for a stoichiometric hydrogen-air mixture obtained by considering the temperature dependency of species enthalpies. The detailed chemistry of the present calculation was from Ref. [27]. It is observed that the explosive mode (λ_{exp}) exists before ignition and crossovers to become a decaying mode after the ignition point, such that the mixture becomes non-explosive. The location where the positive mode crosses zero, referred to as the crossover point, can be defined as the ignition point. Interestingly, the

ignition point obtained in this manner is close to the inflection point on temperature profile, which has been widely accepted as the ignition point in previous literature.

The second example of CEMA involves a direct numerical simulation (DNS) of a turbulent lifted ethylene jet flame in heated coflow which was performed in a three-dimensional slot-burner configuration [30]. As a brief review of the conditions for the DNS, the inlet fuel jet volumetrically consists of 18% ethylene and 82% nitrogen under atmospheric pressure and at a temperature of 550K with a jet velocity of 204m/s. The air coflow is at 1550K with a velocity of 20m/s. The jet Reynolds number is 10,000 based on the slot width, H = 2mm. The size of the computational domain is $15H \times 20H \times 3H$ in the streamwise (x), transverse (y) and spanwise (z) directions, respectively. The compressible Navier–Stokes, species continuity and total energy equations were solved using the Sandia DNS code S3D [31]. A 22-species reduced ethylene mechanism was used to reduce the computation cost of the DNS. Navier-Stokes characteristic boundary conditions (NSCBC) and improved inflow/outflow boundary conditions were used to prescribe the boundary conditions in the x- and y-directions [32-35]. Periodic boundary conditions were used in the z-direction. More detailed information of the DNS can be found in Ref [30].

It is noted that the CEMA in ref. [30] was performed using the analytic Jacobian for the 32-species skeletal mechanism, in which the QSS species concentrations were reconstructed using the algebraic QSS equations from the major species concentrations transported in the DNS. In the present work, the analytic Jacobian of the skeletal mechanism was wrapped using the following equations such that the analytic Jacobian for the reduced mechanism can be directly evaluated from the major species

concentrations in the reduced mechanism. In the following derivations, the concentrations of the QSS species are denoted as $\boldsymbol{C}_m$, and the concentrations of the major species are denoted as $\boldsymbol{C}_n$:

$$\dot{\omega}_n = \dot{W}_n(C_n, C_m, T) = \dot{W}_n(C_n, C_m(C_n, T), T) = \dot{\omega}_n(C_n, T) \quad \textbf{(3.2.1)}$$

The column of the Jacobian for the reduced mechanism can be then computed using chain rule:

$$\left.\frac{\partial \dot{\omega}_n}{\partial C_n}\right|_T = \left.\frac{\partial \dot{\omega}_n}{\partial C_n}\right|_{C_m,T} + \left.\frac{\partial \dot{\omega}_n}{\partial C_m}\right|_{C_n,T} \left.\frac{\partial C_m}{\partial C_n}\right|_T$$

$$\left.\frac{\partial \dot{\omega}_n}{\partial T}\right|_{C_n} = \left.\frac{\partial \dot{\omega}_n}{\partial T}\right|_{C_n,C_m} + \left.\frac{\partial \dot{\omega}_n}{\partial C_m}\right|_{C_n,T} \left.\frac{\partial C_m}{\partial T}\right|_{C_n} \quad \textbf{(3.2.2)}$$

Since the production rates of QSS species are zero based on the QSS approximations, we have:

$$d\dot{\omega}_m = 0, \qquad \frac{\partial \dot{\omega}_m}{\partial C_n} dC_n + \frac{\partial \dot{\omega}_m}{\partial C_m} dC_m + \frac{\partial \dot{\omega}_m}{\partial T} dT = 0 \quad \textbf{(3.2.3)}$$

Consequently, the second multiplier of the second term in equation set (3.2.2) can be obtained from the above equation:

$$\left.\frac{\partial C_m}{\partial C_n}\right|_T = -\left(\frac{\partial \dot{\omega}_m}{\partial C_m}\right)^{-1} \frac{\partial \dot{\omega}_m}{\partial C_n}$$

$$\left.\frac{\partial C_m}{\partial T}\right|_{C_n} = -\left(\frac{\partial \dot{\omega}_m}{\partial C_m}\right)^{-1} \frac{\partial \dot{\omega}_m}{\partial T} \quad \textbf{(3.2.4)}$$

The computation of the Jacobian of the reduced mechanism in (3.3.1.2) is hereby complete.

$$\left.\frac{\partial \dot{\omega}_n}{\partial C_n}\right|_T = \left.\frac{\partial \dot{\omega}_n}{\partial C_n}\right|_{C_m,T} - \left.\frac{\partial \dot{\omega}_n}{\partial C_m}\right|_{C_n,T} \times \left(\frac{\partial \dot{\omega}_m}{\partial C_m}\right)^{-1} \times \frac{\partial \dot{\omega}_m}{\partial C_n}$$

$$\left.\frac{\partial \dot{\omega}_n}{\partial T}\right|_{C_n} = \left.\frac{\partial \dot{\omega}_n}{\partial T}\right|_{C_n,C_m} - \left.\frac{\partial \dot{\omega}_n}{\partial C_m}\right|_{C_n,T} \times \left(\frac{\partial \dot{\omega}_m}{\partial C_m}\right)^{-1} \times \frac{\partial \dot{\omega}_m}{\partial T} \quad \textbf{(3.2.2)}$$

Figure 7 shows the reciprocal time scale of the CEM calculated with analytic Jacobian for the reduced mechanism for the 2-D spanwise slice ($z = 0$) of the DNS results in ref. [30]. The unburned/explosive mixtures are shown in red and burned/non-explosive mixtures are in blue. The transition layer between the burned (red) and unburned (blue) mixture is therefore a (partially) premixed flame front, as discussed in [23]. When no CEM exists in the mixture, the least negative chemical modes are shown instead of CEM. The flame fronts detected by CEMA are shown with white isoline. Furthermore, these results which are based on the CEMA of the reduced mechanism, are in complete agreement with those of the skeletal mechanism [1].

3.3. CEMA for Counterflow Flames

Combustion phenomena are highly nonlinear due to the nonlinear Arrhenius reaction rates. In particular, steady sate combustion is frequently characterized by the "S"-curves, which consist of an upper branch, associated with strongly burning flames, a lower branch, or weakly reacting flames not identifiable by experiments, and a middle branch which is typically unstable. These branches are connected by turning points which features singular Jacobian [36-37]. In the present study, 1-D opposed-flow flames will be selected for flame diagnostics with CEMA, considering that the counterflow flame is frequently used in combustion research, e.g. for the study of flame dynamics and

validation of chemical kinetics. Figure 8 shows the configuration of a counterflow diffusion flames [25], where the fuel and oxidizer exit from the opposite nozzles and the flow diverges as approaching the stagnation plane in the domain center. The steady state strongly burning flame typically will be established near the stagnation plane, and extinction will occur if the strain rate keeps on being increased.

OPPDIF is a CHEMKIN application to simulate steady state counterflow flames [25]. To obtain the "S" curve using OPPDIF, one can first establish a solution on the upper branch, starting from a rough initial guess, and then march along the curve toward the turning point. However, difficulty arises as the solution approaches the turning point because of the singularity of the Jacobian matrix of the governing equations. Such difficulty therefore motivated the change in the OPPDIF code to swap the coordinate for the marching when getting close to the turning points. To swap the coordinate for OPPDIF, temperature at the stagnation plane will be fixed and the inlet velocities will be set as dependent variables instead, such that the Jacobian for the revised equations and boundary conditions is no longer singular at the turning point. The equations and boundary conditions for the revised OPPDIF code are shown in the following pages.

The configuration shown in Fig. 8 produces an axisymmetric flow field with a stagnation plane between the nozzles. At steady-state, the original governing equations for the opposed-flow are given in [25]:

Continuity:

$$\frac{\partial(\rho u)}{\partial x} + \frac{1}{r}\frac{\partial(\rho v r)}{\partial r} = 0 \qquad \textbf{(3.3.1)}$$

where ρ is the mixture density, u and v are the axial and radial velocity components, respectively, and r, and x are the radial and axial directions, respectively. If one further defines variables F(x) and G(x) as:

$$G(x) = -\frac{\rho v}{r}, F(x) = \frac{\rho u}{2} \quad \textbf{(3.3.2)}$$

Then equation (3.3.1) becomes

$$G(x) = \frac{dF(x)}{dx} \quad \textbf{(3.3.3)}$$

Following Kee, et al [36] the pressure gradient equation satisfies

$$H = \frac{1}{r}\frac{\partial p}{\partial r} = constant \quad \textbf{(3.3.4)}$$

where p is pressure.

Momentum equation in r-direction:

$$H - 2\frac{d}{dx}\left(\frac{FG}{\rho}\right) + \frac{3G^2}{\rho} + \frac{d}{dx}\left[\mu\frac{d}{dx}\left(\frac{G}{\rho}\right)\right] = 0 \quad \textbf{(3.3.5)}$$

where μ is the dynamic viscosity.

Energy equation:

$$\rho u\frac{dT}{dx} - \frac{1}{\bar{c_p}}\frac{d}{dx}\left(\lambda\frac{dT}{dx}\right) + \frac{\rho}{\bar{c_p}}\sum_{k=1}^{KK} c_{p_k} Y_k V_k \frac{dT}{dx} + \frac{1}{\bar{c_p}}\sum_{k=1}^{KK} h_k \dot{\omega}_k = 0 \quad \textbf{(3.3.6)}$$

where T is temperature, $\bar{c_p}$ is the mixture averaged specific heat capacity at constant pressure, and λ is the mixture averaged heat conductivity. The subscript k indicates the

*k*th species, and c_{p_k}, Y_k, V_k, h_k, and $\dot{\omega}_k$ are the specific heat capacity at constant pressure, mass fraction, diffusive velocity, specific enthalpy, and chemical production rate of the *k*th species, respectively. It is noted that V_k can be computed by either the multicomponent or the mixture-averaged diffusion models [25].

Species conservation equation:

$$\rho u \frac{dY_k}{dx} + \frac{d}{dx}\left(\rho Y_k V_k\right) - \dot{\omega}_k W_k = 0 \qquad \textbf{(3.3.7)}$$

where W_k is the Molecular weight of the k_{th} species.

Boundary conditions at fuel the side,$(x = 0)$*, and the oxidizer side* $(x = L)$*:*

$$F(x=0) = \frac{\rho_F u_F}{2}; G(x=0) = 0; T(x=0) = T_F;$$

$$H(x=0) = constant; Y_k(x=0) = Y_{k_F}$$

$$F(x=L) = \frac{\rho_O u_O}{2}; G(x=L) = 0; T(x=L) = T_O; \qquad \textbf{(3.3.8)}$$

$$G(x=L) = \frac{dF(x=L)}{dx}; Y_k(x=L) = Y_{k_O}$$

where L is the distance between the nozzles. The subscripts *F* and *O* indicates the fuel and the oxidizer boundaries, respectively.

The differential equations and boundary conditions in Eqs. (3.3.3-3.3.8) then form a closed boundary value problem for the dependent variables. OPPDIF calls the TWOPNT [38] for solving the boundary value problem using the Newton iteration method.

To swap the coordinate in the above equations, the differential equations in (3.3.3-3.3.7) will be used in conjunction with the following revised boundary conditions.

First, the stagnation plane is fixed at the domain center, e.g.:

$$at\ x = \frac{L}{2}, \qquad v = 0 \tag{3.3.9}$$

As such, the boundary condition for axial velocity at the fuel boundary can be replaced with (3.3.9). Furthermore, the inlet velocities at both boundaries have been removed from the boundary conditions and were included as an independent variable in the equation set,

Secondly, the temperature at the stagnation plane, denoted by T^*, is specified as a given value:

$$T = T^*, \text{ at } at\ x = x^*, \tag{3.3.10}$$

such that it is removed from the set of variables in the equation set and the total number of variables, equations, and boundary conditions remain the same as those in the original OPPDIF. Furthermore, a residence time, τ, for the flow is defined as

$$\tau = \frac{L}{V_F} \tag{3.3.11}$$

When marching on the upper branch using the original equations, one can reduce the residence time τ, which is equivalent to increasing the strain rate, by a small step size $\Delta\tau$ and then solve the flow field. While when marching around the turning point using the revised equations, one can increase the temperature at the stagnation point by a small value ΔT^*, and then solve for the inlet velocities and other variables in the flow field. In general, the calculations converge more easily for smaller values of ΔT^*. Here ΔT^* is set to 3K in most of the following marching. The revised OPPDIF was then used to obtain

solutions for various fuels as shown in Figs. 9-11, for hydrogen, methane, and ethylene, respectively. The results from the revised OPPDIF were then compared with that from the original version to ensure that the solutions from both versions are identical to each other.

The solutions on different branches of the "S"-curves obtained with the original and the revised OPPDIF were then employed for CEMA. Figures 12-14 show temperature profiles and the reciprocal time scales of the chemical explosive mode as functions of the axial location *x*. Figure 12 shows a point on the upper branch of the "S"-curve for a strongly burning methane-air flame with a strain rate of 12.59 (s^{-1}), calculated with GRI-Mech 1.2 [39]. It is seen in Fig. 12b that no explosive mode is present at this point. Figure 13 shows a point near the upper turning point with a strain rate of 79.445 (s^{-1}). It is seen that CEM is present in this near-extinction flame near the reaction zone. Figure 14 shows a case on the middle branch below the turning point with strain rate of 102.615 (s^{-1}). It is seen that CEM is also present near the reaction zone. Therefore it is shown that CEM exists in near-extinction counterflow diffusion flames, similar to the observations made for near-extinction PSR flames [1].

3.4. Explosive Mode Analysis (EMA)

While CEMA is focused on the chemical property of the local mixture, eigenanalysis for the full Jacobian can provide such information as the stability of the system. Therefore it is of interest to extend CEMA to the full Jacobian in the present study.

After discretization, the governing equation for a general convective-diffusive-reactive system can be expressed in the form of Eq. (3.1.1). The full Jacobian matrix J can

therefore be divided to a chemical Jacobian and a non-chemical Jacobian, denoted as $\mathbf{J_\omega}$, and $\mathbf{J_s}$, respectively:

$$\frac{dg}{dt} = J \,.\, g(y)\,, \qquad J = \frac{dg}{dy} = J_\omega + J_s\,, \tag{3.4.1}$$

$$\boldsymbol{J_\omega} = \frac{\partial \boldsymbol{\omega}}{\partial \boldsymbol{y}}\,, and\, \boldsymbol{J_s} = \frac{\partial \boldsymbol{s}}{\partial \boldsymbol{y}} \tag{3.4.2}$$

The real part of the eigenvalues of the full Jacobian indicates the reciprocal time scale of the corresponding eigenmode, which can be either negative or positive. A large negative value indicates fast decaying mode [24], which will become exhausted in a transient period and can be described by an algebraic equation [2]. A positive eigenvalue of the full Jacobian indicates that the system is unstable, since any small perturbation will be magnified in the direction of the explosive eigenmode. The eigenmode associated with a positive eigenvalue of the full Jacobian is therefore an explosive mode. The state where an explosive mode crosses zero indicates the transition from a stable to an unstable system, and such a state is known as a bifurcation point.

The eigenmode of the full Jacobian consists of the contributions from the chemical source term and the non-chemical source term. The eigenvalues of $\mathbf{J_s}$ in a diffusive system are typically all negative due to the dissipative nature of the diffusion processes. Therefore, if an eigenmode of the full Jacobian is positive, a CEM should be present and attributes primarily to the positive eigenmode of the full Jacobian. By analyzing the competition between the chemical modes and diffusive modes, explosive

mode analysis (EMA) effectively considers all the source terms in the right hand side of equation (3.4.1) and provides information for explaining the near-limit system behaviors.

To demonstrate the usage of EMA in analyzing near-limit flame behaviors, Figure 15 shows the explosive mode of the entire governing equation of a stoichiometric H_2-Air mixture in a steady state PSR under atmospheric pressure and an inlet temperature of 900K. For comparison, the profile of residence time vs. temperature in logarithmic scale is also plotted. The profile includes the physically stable upper branch of the combustion S-curve, which is connected to the unstable middle branch at the extinction point. As can be seen from Figure 15, in the regime with large residence times and high temperatures, the system is near chemical equilibrium and almost all the reactants have been consumed. Therefore explosive mode does not exist on the upper branch of the S-curve far away from the extinction point. By marching toward the turning point on the upper branch, the concentrations of reactants increase due to the reduced residence time for chemical reaction and thus lowered temperature, such that the mixture eventually becomes explosive close to the extinction point. The chemical explosive mode near the extinction point then attributes to an increasing eigenvalue in the full Jacobian. At the extinction point, the chemical explosive mode is balanced by the loss, such that the eigenvalue of the full Jacobian crosses zero, and the full Jacobian becomes singular. i.e.:

$$\lambda_{exp} \approx \lambda_c + \lambda_s \qquad \textbf{(3.4.3)}$$

Below the turning point, the chemical explosive mode become even stronger while the loss processes become relatively slower, as such the eigenvalue of the full Jacobian becomes positive and the system becomes unstable.

The contribution of the mixing and chemical source term is further shown in Figure 16. It is observed that the crossover point of λ_c is very close to the singularity point of explosive mode, which indicates that chemistry balances mixing at the turning point and the chemical explosive mode is the primary factor driving λ to cross zero at the turning point.

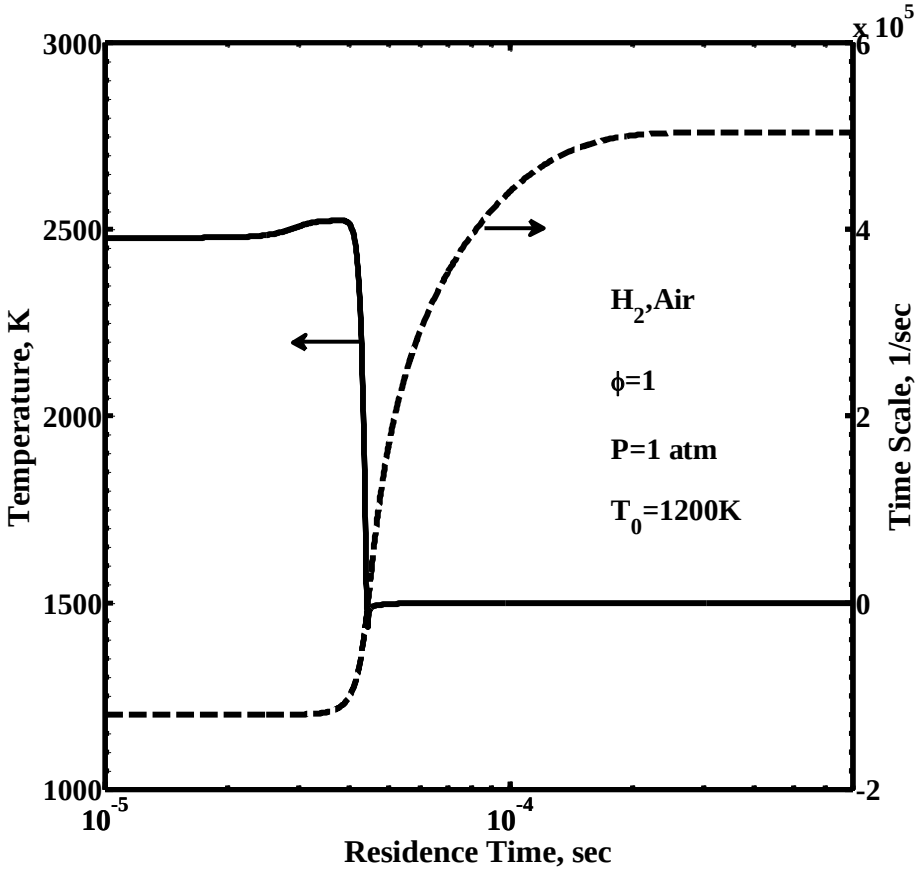

Figure 6. Temperature profile and reciprocal time scale, λ_{exp}, of the least negative chemical mode in auto-ignition of a stochiometric hydrogen- air mixture under constant pressure of 1atm and an initial temperature of 1200 K.

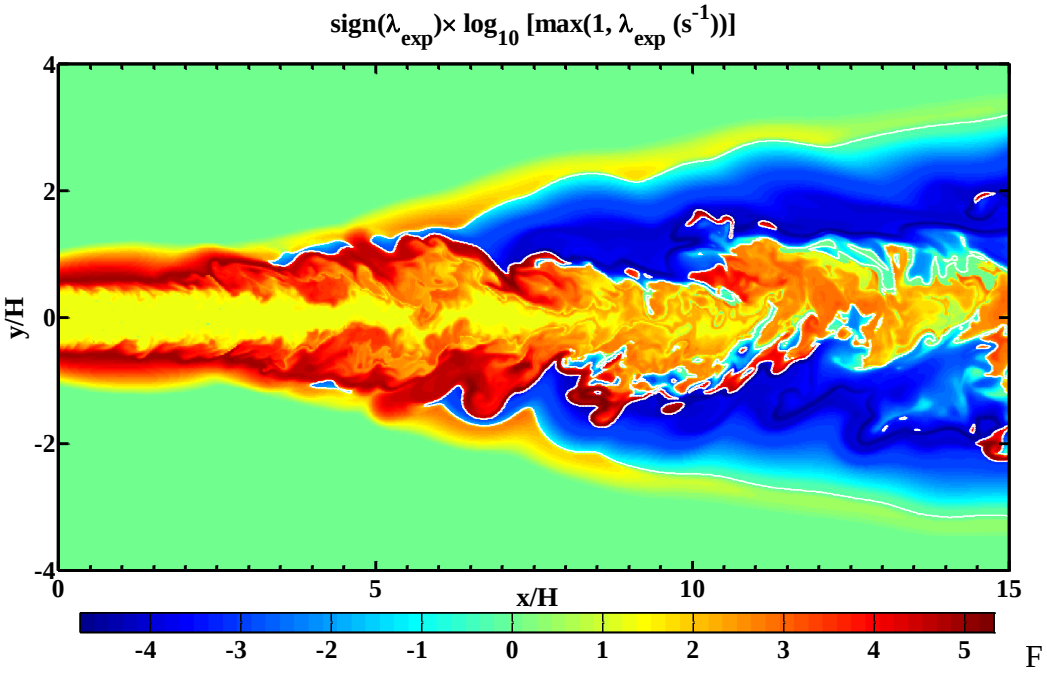

Figure 7. Spatial distribution of the time scale of local chemical explosive modes from a span wise slice from DNS of an Ethylene jet issuing into preheated air. A negative value of λ_{exp} is the eigenvalue associated with the slowest decaying mode in a non-explosive mixture. The boundary between non-explosive and explosive regions is delineated by a white isocontour at $\lambda_{exp} = 0$

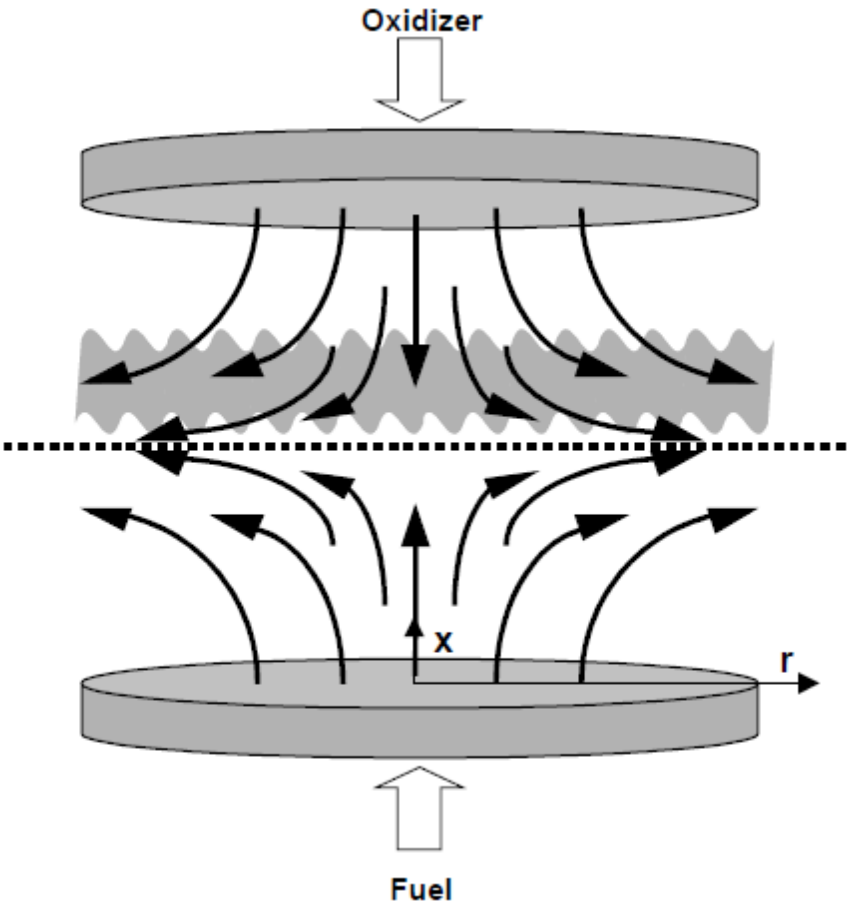

Figure 8. Configuration of the axisymmetric opposed-flow diffusion flame. The dashed line represents the stagnation plane; the shaded region suggests the flame (image from [25]).

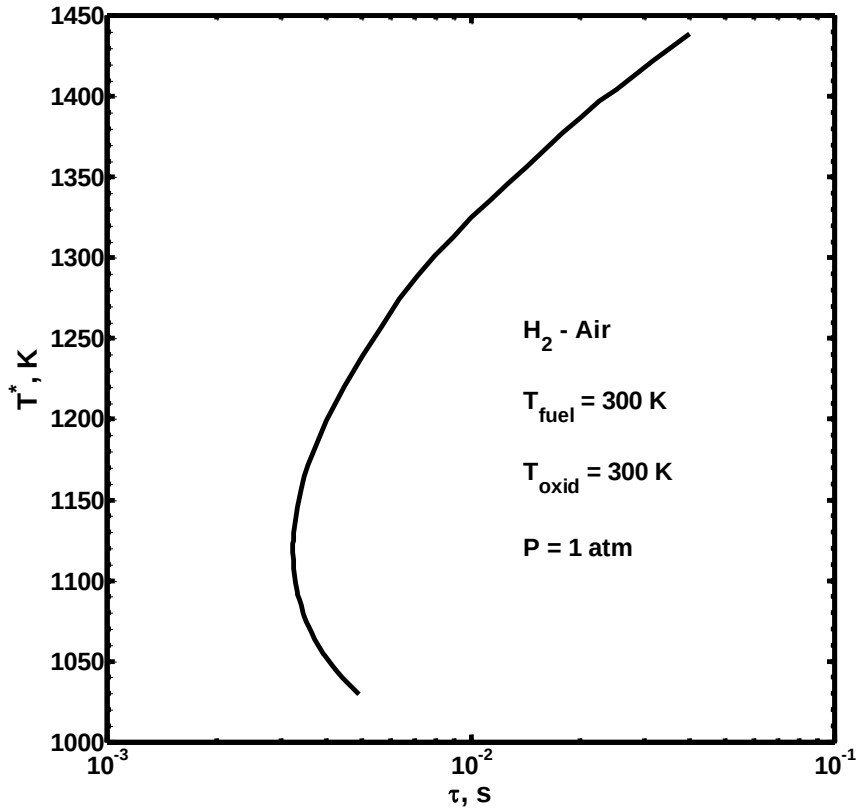

Figure 9. Extinction curve of hydrogen diluted with 80 % nitrogen volumetrically on the fuel side and air on the oxidizer size for opposed flow configuration.

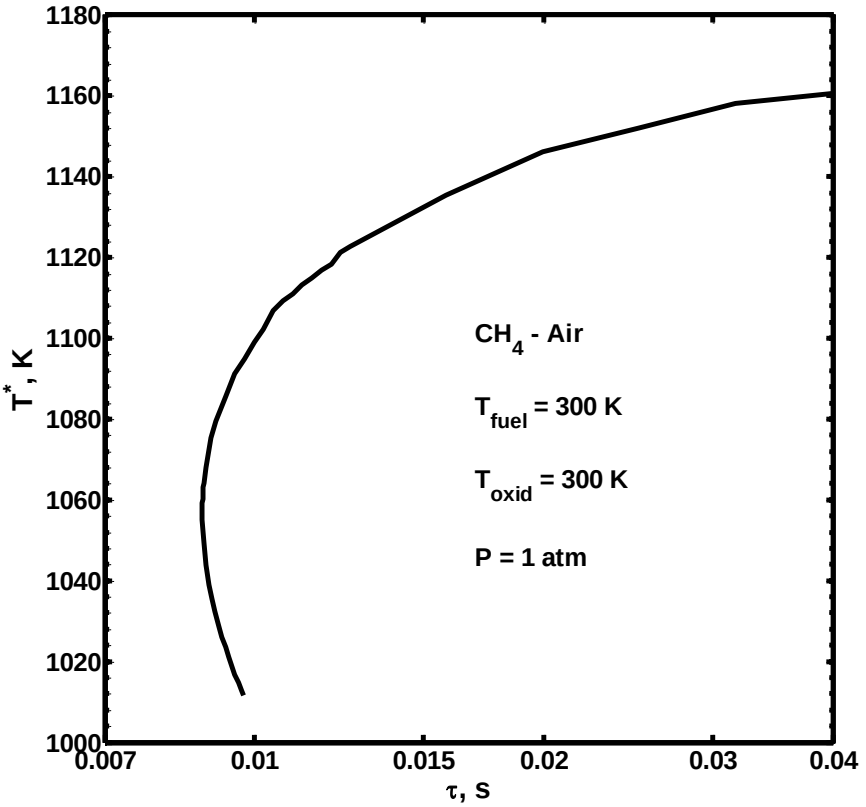

Figure 10. S-curve response of steady methane/air diffusion flame with GRI-1.2[39]. Methane is diluted with 50 % nitrogen volumetrically on the fuel side.

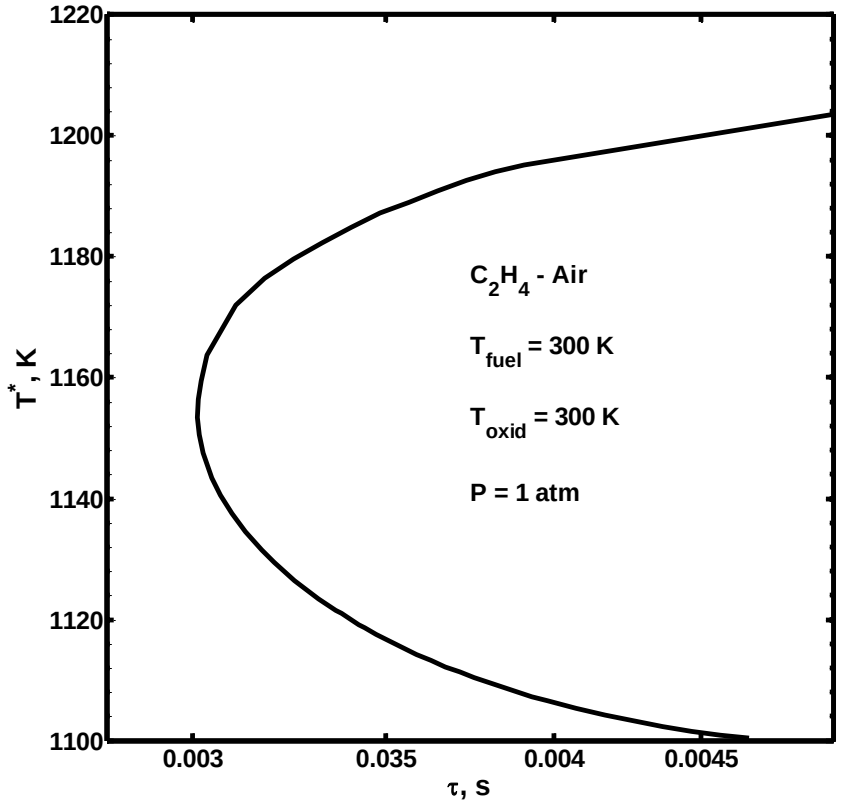

Figure 11.S-curve of steady ethylene /air diffusion flames with a reduced mechanism. Ethylene is diluted with 50 % nitrogen volumetrically on the fuel side[40].

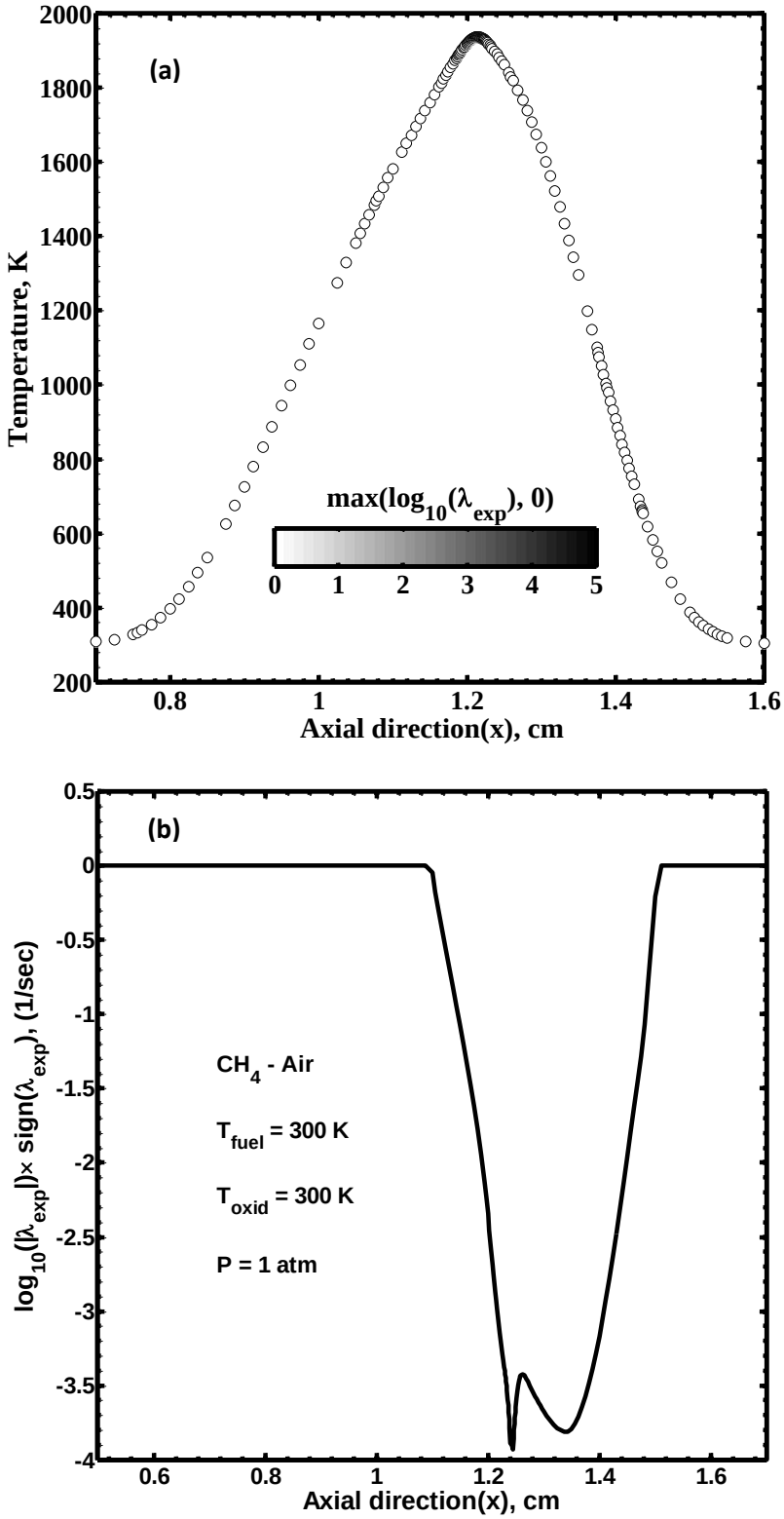

Figure 12. a) Temperature profile, the color of the circles represents the reciprocal time scale of CEM, and b) CEM at a point on the upper branch of the S-curve far away from the extinction point.

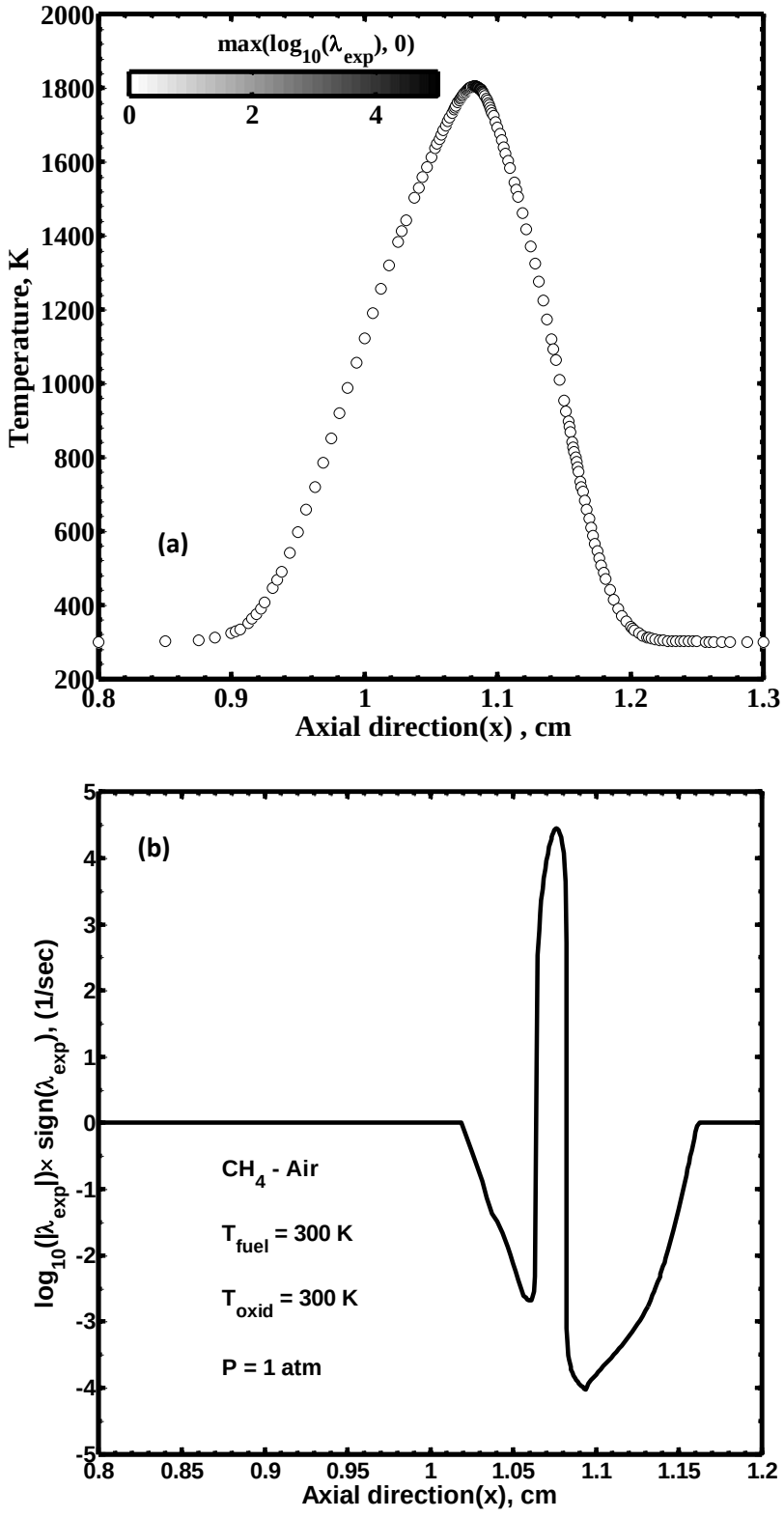

Figure 13. a) Temperature profile; the color of the circles represents the reciprocal time scale of CEM, and b) chemical explosive mode at a point on the upper branch of S-curve close to extinction point.

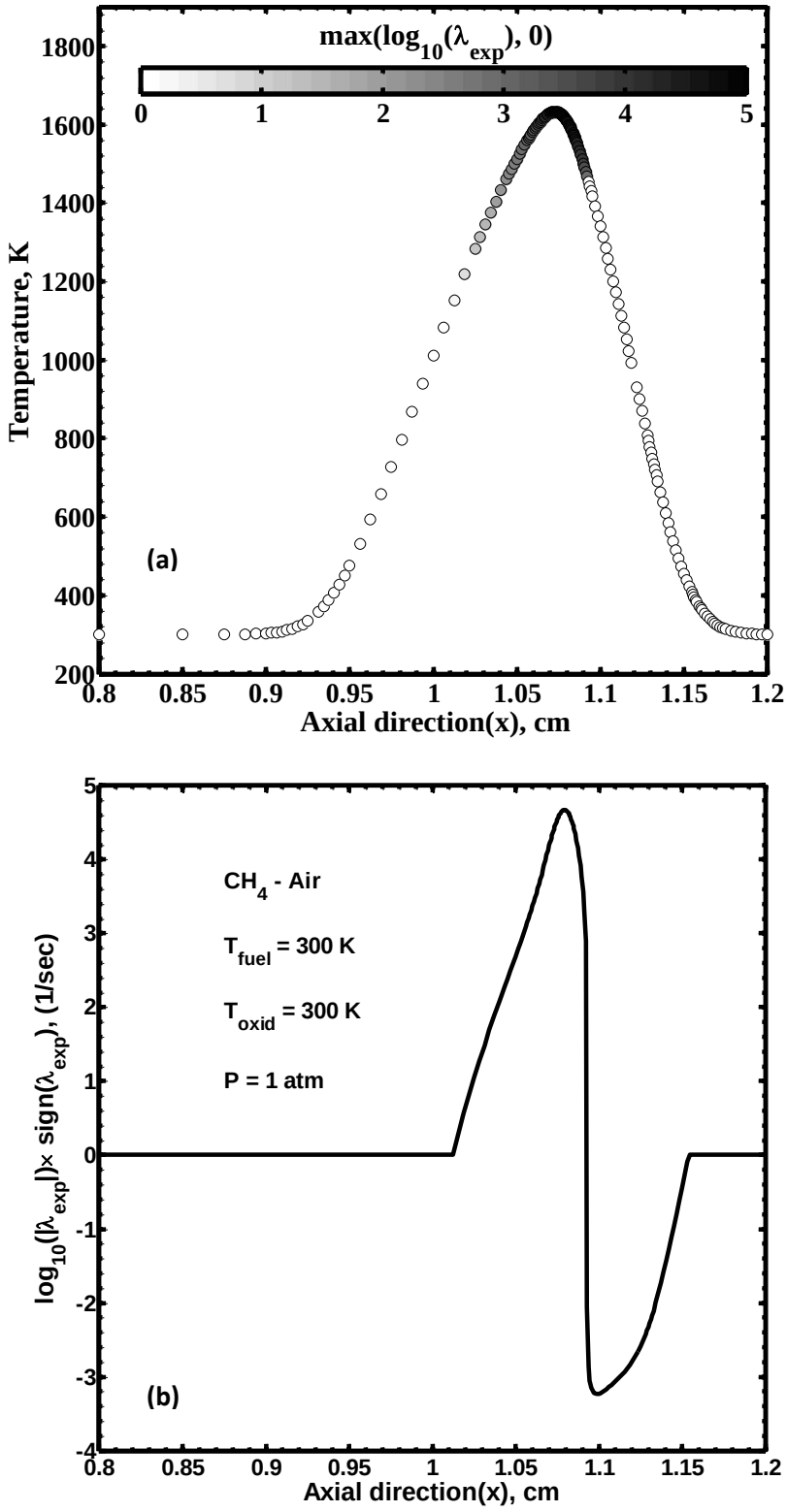

Figure 14. a) Temperature profile; the color of the circles represents the reciprocal time scale of the CEM, and b) chemical explosive mode at a point on the middle branch of S-curve below the extinction point.

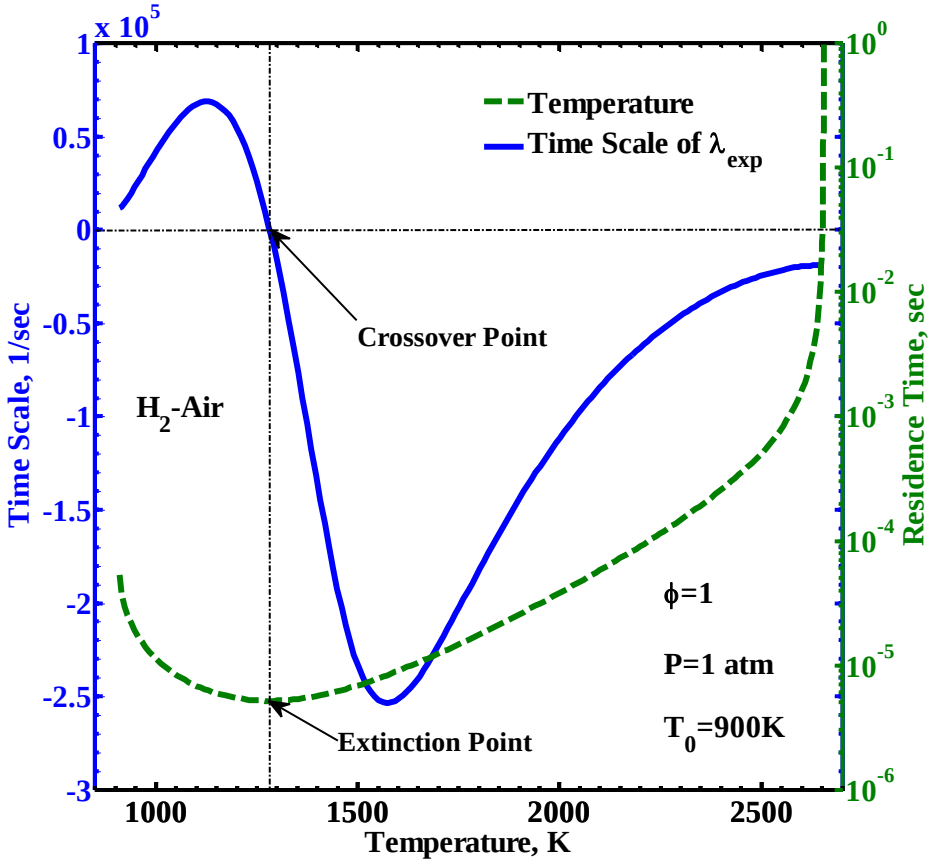

Figure 15. Time scale of the explosive mode, and residence time vs. temperature in a steady-state perfectly stirred reactor with stochiometric hydrogen-air mixture under atmospheric pressure and an inlet temperature of 900K.

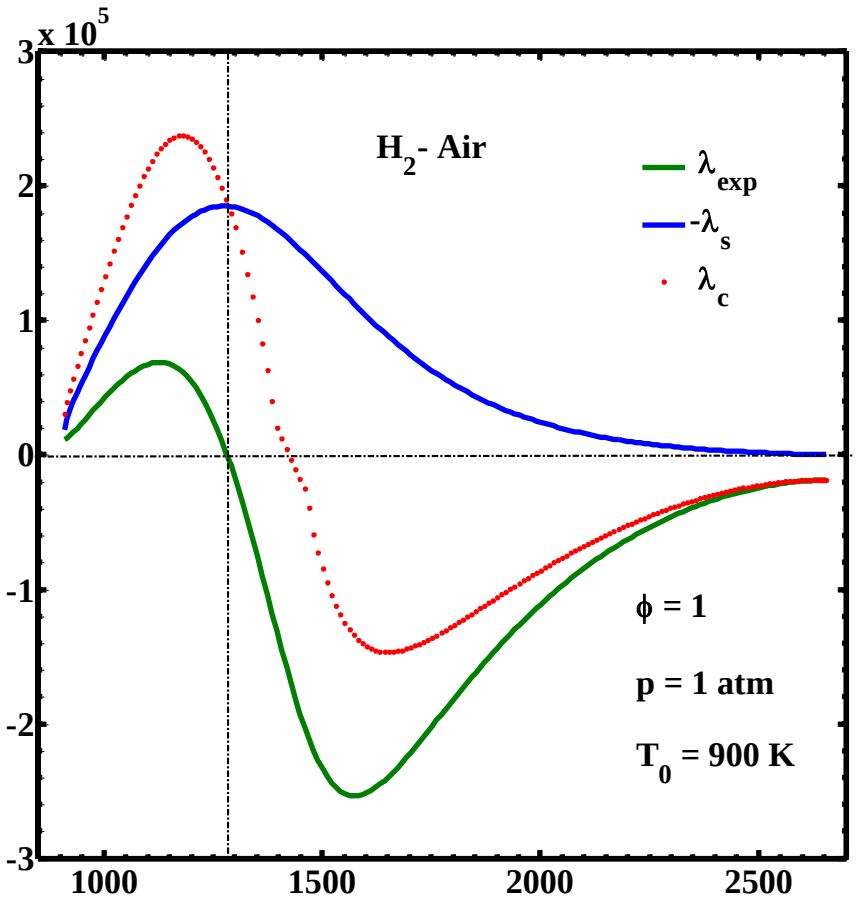

Figure 16. Contribution of Chemistry and loss in the evolvement of the explosive mode in a steady-state perfectly stirred reactor with stochiometric hydrogen-air mixture under atmospheric pressure and an inlet temperature of 900K.

Chapter 4. Concluding Remarks

In summary, analytical Jacobian has been developed for detailed chemistry and 0-D applications of Senkin and PSR. Effort was also made on deriving the analytic Jacobian for the counterflow flames, while this will be investigated in the further work. The analytic Jacobian was shown to be both accurate and efficient, as required by CEMA and EMA to capture the zero-crossover of the eigenvalues.

The analytical Jacobian was then utilized to study the role of explosive modes in flame diagnostics especially for the detection of ignition, and extinction point in Senkin and PSR. The interaction between the mixing processes and CEM was further studied for perfectly stirred reactors. Analytic Jacobian was developed for reduced mechanism involving QSS species, and CEMA was then performed for visualizing the structure of a lifted ethylene jet flame into heated coflowing air simulated by DNS.

The OPPDIF code for steady state 1-D counterflow flame simulation was revised to allow the marching along the "S"-curves around the turning points. The solution from the revised OPPDIF code was then employed for CEMA. It was found that no CEM is present for strongly burning diffusion flames on the upper branches, while CEM appears as the flame approaches the extinction point. This observation is consistent with that observed in PSR.

CEMA was then extended to EMA by using the full Jacobian of the governing equations that consists of the contributions from the chemical source terms and the mixing term. It was shown that CEM is the dominant factor driving the eigenvalue of the full Jacobian crossing zero, subsequently changing the stability of the system, while

mixing plays a dissipative role and balances the CEM at the turning points. More detailed analysis of the explosive modes of the system, e.g. the contribution from a species or a reaction to the explosive modes can be an interesting direction to extend the present work in the future.

Appendix: Analytical Jacobian Derivation for the chemical part of the governing equations in SENKIN, PSR, and OPPDIF

List of Symbols

C_i	Molar concentration of the i_{th} species
T	Temperature
P	Pressure
ρ	Mixture density
Y_i	Mass fraction of the i_{th} species
W_i	Molecular weight of the i_{th} species
$\bar{W}$	Mean molecular weight of a mixture
KK	Total number of species
$\dot{\omega}_i$	Chemical production rate of the i_{th} species
Ru	Universal gas constant
H_i	Molar enthalpy of the i_{th} species
$\bar{c_p}$	Mean specific heat capacity at constant pressure
c_{p_i}	Specific heat capacity at constant pressure of the i_{th} species
c_{v_i}	Specific heat capacity at constant volume of the i_{th} species

Species molar concentrations can change by either temperature or species mass fractions as follows:

$$\left(\frac{\partial C_i}{\partial T}\right)_{P,Y_i} = \frac{\partial}{\partial T}\left(\frac{\rho Y_i}{W_i}\right)_{P,Y_i} = \frac{Y_i}{W_i}\left(\frac{\partial \rho}{\partial T}\right)_{P,Y_i} = -\frac{\rho Y_i}{T W_i}$$

$$\left(\frac{\partial C_i}{\partial Y_j}\right)_{P,T,Y_{i\neq j}} = \frac{\partial}{\partial Y_j}\left(\frac{\rho Y_i}{W_i}\right)_{P,T,Y_{i\neq j}} = \frac{1}{W_i}\left[Y_i\left(\frac{\partial \rho}{\partial Y_j}\right)_{P,T,Y_{i\neq j}} + \rho\left(\frac{\partial Y_i}{\partial Y_j}\right)_{P,T,Y_{i\neq j}}\right]$$

$$= \frac{1}{W_i}\left[Y_i\left(\frac{\partial \rho}{\partial Y_j}\right)_{P,T,Y_{i\neq j}} + \rho\left(\frac{\partial Y_i}{\partial Y_j}\right)_{P,T,Y_{i\neq j}}\right] = \begin{cases} -\dfrac{\rho Y_i \bar{W}}{W_j} + \rho & i = j \\ -\dfrac{\rho Y_i \bar{W}}{W_j} & i \neq j \end{cases}$$

Mixture average density changes with temperature and species mass fractions as follow:

$$\left(\frac{\partial \rho}{\partial T}\right)_{P,Y_i} = \left(\frac{\partial}{\partial T}\left(P\bar{W}/Ru\,T\right)\right)_{P,Y_i} = -\frac{P\bar{W}}{Ru\,T^2} \times \frac{Y_i}{W_i} = -\frac{\rho}{T}$$

$$\left(\frac{\partial \rho}{\partial Y_j}\right)_{P,T,Y_{i\neq j}} = \left(\frac{\partial}{\partial Y_j}\left(P\bar{W}/Ru\,T\right)\right)_{P,T,Y_{i\neq j}} = \frac{P}{Ru\,T}\left(\frac{\partial \bar{W}}{\partial Y_j}\right)_{P,T,Y_{i\neq j}} = \frac{P}{Ru\,T} \times -\frac{\bar{W}^2}{W_j}$$

$$= -\frac{\rho \bar{W}}{W_j}$$

Mean molecular weight of the mixture which is denoted by $\bar{W}$ can be just changed with temperature as follows:

$$\left(\frac{\partial \bar{W}}{\partial Y_j}\right)_{P,T,Y_{i\neq j}} = \left(\frac{\partial}{\partial Y_j}\left(\frac{1}{\sum_{i=1}^{KK} Y_i/W_i}\right)\right)_{P,T,Y_{i\neq j}}$$

$$= -\left(\frac{\partial}{\partial Y_j}\left(\sum_{i=1}^{KK} Y_i/W_i\right)\right)_{P,T,Y_{i\neq j}} \Bigg/ \left(\sum_{i=1}^{KK} Y_i/W_i\right)^2$$

$$= -\frac{\bar{W}^2}{W_j}$$

Chemical term for the k^{th} species equation is defined by :

$$F(Y_i) = \frac{\dot{\omega}_i \times W_i}{\rho}$$

The derivative of $F(Y_i)$ with respect to temperature is:

$$\left(\frac{\partial F(Y_i)}{\partial T}\right)_{P,Y_i} = \left(\frac{\partial}{\partial T}\left(\frac{W_i \dot{\omega}_i}{\rho}\right)\right)_{P,Y_i} = W_i\left[\frac{1}{\rho}\left(\frac{\partial \dot{\omega}_i}{\partial T}\right)_{P,Y_i} + \dot{\omega}_i\left(\frac{\partial\,(1/\rho)}{\partial T}\right)_{P,Y_i}\right]$$

$$= W_i\left[\frac{1}{\rho}\left(\frac{\partial \dot{\omega}_i}{\partial T}\right)_{P,Y_i} + \frac{\dot{\omega}_i}{T}\right]$$

Where the derivative of the inverse of mixture density with respect to temperature is:

$$\frac{\partial}{\partial T}\left(\frac{1}{\rho}\right)_{P,Y_i} = \left(\frac{\partial}{\partial T}\left(Ru\,T/P\overline{W}\right)\right)_{P,Y_i} = \frac{Ru}{P\overline{W}} = \frac{1}{\rho T}$$

The derivative of $F(Y_i)$ with respect to the mass fraction of species (j) is:

$$\left(\frac{\partial F_i}{\partial Y_j}\right)_{P,T,Y_{i\neq j}} = \left(\frac{\partial}{\partial Y_j}\left(\frac{W_i \dot{\omega}_i}{\rho}\right)\right)_{P,T,Y_{i\neq j}} = W_i\left[\frac{1}{\rho}\left(\frac{\partial \dot{\omega}_i}{\partial Y_j}\right)_{P,T,Y_{i\neq j}} + \dot{\omega}_i\left(\frac{\partial\,(1/\rho)}{\partial Y_j}\right)_{P,T,Y_{i\neq j}}\right]$$

$$= \frac{W_i}{\rho}\left[\left(\frac{\partial \dot{\omega}_i}{\partial Y_j}\right)_{P,T,Y_{i\neq j}} + \frac{\dot{\omega}_i \overline{W}}{W_j}\right]$$

Where the derivative of the inverse of mixture density with respect to species mass fractions is:

$$\frac{\partial}{\partial Y_j}\left(\frac{1}{\rho}\right)_{P,T,Y_{i\neq j}} = \left(\frac{\partial}{\partial Y_j}\left(Ru\,T/P\overline{W}\right)\right)_{P,T,Y_{i\neq j}} = \frac{Ru\,T}{P}\left(\frac{\partial}{\partial Y_j}\left(1/\overline{W}\right)\right)_{P,T,Y_{i\neq j}} = \frac{\overline{W}}{\rho W_j}$$

And the derivative of the inverse of mixture average molecular weight with respect to species mass fractions can be obtained as follows:

$$\left(\frac{\partial}{\partial Y_j}\left(\frac{1}{\bar{W}}\right)\right)_{P,T,Y_{i\neq j}} = \left(\frac{\partial}{\partial Y_j}\left(\sum_{i=1}^{KK}\frac{Y_i}{W_i}\right)\right)_{P,T,Y_{i\neq j}} = \frac{1}{W_j}$$

Chemical part of energy equation is defined by:

$$F_{Energy} = -\frac{\sum_{i=1}^{KK}\dot{\omega}_i H_i}{\rho\bar{c_p}}$$

The derivative of F_{Energy} with respect to temperature is:

$$\left(\frac{\partial F}{\partial T}\right)_{P,Y_i} = -\left(\frac{\partial}{\partial T}\left(\frac{\sum_{i=1}^{KK}\dot{\omega}_i H_i}{\rho\bar{c}_p}\right)\right)_{Y_i}$$

$$= -\sum_{i=1}^{KK}\dot{\omega}_i H_i \times \left(\frac{\partial}{\partial T}\left(\frac{1}{\rho\bar{c}_p}\right)\right)_{P,Y_i} - \frac{1}{\rho\bar{c}_p}\times\sum_{i=1}^{KK}H_i\left(\frac{\partial\dot{\omega}_i}{\partial T}\right)_{P,Y_i} - \frac{1}{\rho\bar{c}_p}\times\sum_{i=1}^{KK}\dot{\omega}_i\left(\frac{\partial H_i}{\partial T}\right)_{E_i}$$

$$= \frac{\sum_{i=1}^{KK}\dot{\omega}_i H_i}{\left(\sum_{i=1}^{KK}C_i c_{v_i}\right)^2}\times\sum_{i=1}^{KK}C_i\left(\frac{\partial c_{v_i}}{\partial T}\right)_{Y_i} - \frac{1}{\sum_{i=1}^{KK}C_i c_{v_i}}\times\sum_{i=1}^{KK}H_i\left(\frac{\partial\dot{\omega}_i}{\partial T}\right)_{Y_i} - \frac{1}{\sum_{i=1}^{KK}C_i c_{v_i}}\times\sum_{i=1}^{KK}c_{p_i}\dot{\omega}_i$$

Similarly, The derivative of F_{Energy} with respect to mass fraction of species (j) can be computed as follows:

$$\left(\frac{\partial F}{\partial Y_j}\right)_{P,T,Y_{i\neq j}} = -\left(\frac{\partial}{\partial Y_j}\left(\frac{\sum_{i=1}^{KK}\dot{\omega}_i H_i}{\rho\bar{c}_p}\right)\right)_{P,T,Y_{i\neq j}}$$

$$= -\sum_{i=1}^{KK}\dot{\omega}_i H_i \times \left(\frac{\partial}{\partial Y_j}\left(\frac{1}{\rho\bar{c}_p}\right)\right)_{P,T,Y_{i\neq j}} - \frac{1}{\rho\bar{c}_p}\times\sum_{i=1}^{KK}H_i\left(\frac{\partial\dot{\omega}_i}{\partial Y_j}\right)_{P,T,Y_{i\neq j}}$$

$$= -\sum_{i=1}^{KK}\dot{\omega}_i H_i \times \left(\frac{\partial}{\partial Y_j}\left(\frac{1}{\sum_{i=1}^{KK}C_i c_{p_i}}\right)\right)_{P,T,Y_{i\neq j}} - \frac{1}{\sum_{i=1}^{KK}C_i c_{p_i}}\times\sum_{i=1}^{KK}H_i\left(\frac{\partial\dot{\omega}_i}{\partial Y_j}\right)_{P,T,Y_{i\neq j}} =$$

$$\frac{\sum_{i=1}^{KK}\dot{\omega}_i H_i}{\left(\sum_{i=1}^{KK}C_i c_{p_i}\right)^2}\times\sum_{i=1}^{KK}c_{p_i}\left(\frac{\partial C_i}{\partial Y_j}\right)_{P,T,Y_{i\neq j}} - \frac{1}{\sum_{i=1}^{KK}C_i c_{p_i}}\times\sum_{i=1}^{KK}H_i\left(\frac{\partial\dot{\omega}_i}{\partial Y_j}\right)_{P,T,Y_{i\neq j}}$$

References

[1]. Z. Luo; C. S. Yoo; E. S. Richardson; J. H. Chen; C. K. Law; T. Lu, *"Chemical explosive mode analysis for a turbulent lifted ethylene jet flame in highly-heated coflow"*. Combustion and Flame, Article in Press (2011)

[2]. U. Maas; S. B. Pope, *"Simplifying chemical kinetics: intrinsic low-dimensional manifolds in composition space"*. Combustion and Flame 88 (3-4) (1992) 239-264

[3]. S. Lam, *"Using CSP to understand complex chemical kinetics"*. Combustion Science and Technology 89 (5) (1993) 375-404

[4]. S. Lam; D. Goussis, *"The CSP method for simplifying kinetics"*. International Journal of Chemical Kinetics 26 (4) (1994) 461-486

[5]. S. Lam, *"Singular perturbation for stiff equations using numerical methods "*. Recent advances in the aerospace sciences, Plenum Press, New York (1985)

[6]. S. Lam, *"Reduced chemistry-diffusion coupling"*. Combustion Science and Technology 179 (4) (2007) 767-786

[7]. A. Massias; D. Diamantis; E. Mastorakos; D. Goussis, *"Global reduced mechanisms for methane and hydrogen combustion with nitric oxide formation constructed with CSP data"*. Combustion Theory and Modelling 3 (2) (1999) 233-257

[8]. A. Massias; D. Diamantis; E. Mastorakos; D. Goussis, *"An algorithm for the construction of global reduced mechanisms with CSP data"*. Combustion and Flame 117 (4) (1999) 685-708

[9]. T. Lu; Y. Ju; C. K. Law, *"Complex CSP for chemistry reduction and analysis"*. Combustion and Flame 126 (1-2) (2001) 1445-1455

[10]. T. Lu; C. K. Law, *"A criterion based on computational singular perturbation for the identification of quasi steady state species: A reduced mechanism for methane oxidation with NO chemistry"*. Combustion and Flame 154 (4) (2008) 761-774

[11]. M. Valorani; F. Creta; D. A. Goussis; J. C. Lee; H. N. Najm, *"An automatic procedure for the simplification of chemical kinetic mechanisms based on CSP"*. Combustion and Flame 146 (1-2) (2006) 29-51

[12]. M. Valorani; D. A. Goussis; F. Creta; H. N. Najm, *"Higher order corrections in the approximation of low-dimensional manifolds and the construction of simplified problems with the CSP method"*. Journal of Computational Physics 209 (2) (2005) 754-786

[13]. D. A. Goussis; M. Valorani, *"An efficient iterative algorithm for the approximation of the fast and slow dynamics of stiff systems"*. Journal of Computational Physics 214 (1) (2006) 316-346

[14]. J. Lee; H. Najm; S. Lefantzi; J. Ray; M. Frenklach; M. Valorani; D. Goussis, *"A CSP and tabulation-based adaptive chemistry model"*. Combustion Theory and Modelling 11 (1) (2007) 73-102

[15]. M. Valorani; H. N. Najm; D. A. Goussis, *"CSP analysis of a transient flame-vortex interaction:: time scales and manifolds"*. Combustion and Flame 134 (1-2) (2003) 35-53

[16]. D. A. Goussis; H. N. Najm, *"Model reduction and physical understanding of slowly oscillating processes: the circadian cycle"*. Multiscale Modeling & Simulation 5 (2006) 1297-1332

[17]. C. Fotache; T. Kreutz; C. Law, *"Ignition of hydrogen-enriched methane by heated air"*. Combustion and Flame 110 (4) (1997) 429-440

[18]. A. Kazakov; M. Chaos; Z. Zhao; F. L. Dryer, *"Computational singular perturbation analysis of two-stage ignition of large hydrocarbons"*. The Journal of Physical Chemistry A 110 (21) (2006) 7003-7009

[19]. A. Zagaris; H. G. Kaper; T. J. Kaper, *"Analysis of the computational singular perturbation reduction method for chemical kinetics"*. Journal of Nonlinear Science 14 (1) (2004) 59-91

[20]. A. Zagaris; H. G. Kaper; T. J. Kaper, *"Two perspectives on reduction of ordinary differential equations"*. Mathematische Nachrichten 278 (12-13) (2005) 1629-1642

[21]. A. Zagaris; H. G. Kaper; T. J. Kaper, *"Fast and slow dynamics for the computational singular perturbation method"*. Multiscale Modeling & Simulation 2 (4) (2004) 613- 638

[22]. T. Lu; C. K. Law, *"Strategies for mechanism reduction for large hydrocarbons: n-heptane"*. Combustion and Flame 154 (1-2) (2008) 153-163

[23]. T. Lu; C. Yoo; J. Chen; C. Law, *"Three-dimensional direct numerical simulation of a turbulent lifted hydrogen jet flame in heated coflow: a chemical explosive mode analysis"*. Journal of Fluid Mechanics 652 (2010) 45-64

[24]. T. F. Lu; M. Wang; C. S. Yoo; C. K. Law, *"A Mode Tracking Method for Flow Classification"*. 6th US National Combustion Meeting, Ann Arbor, Michigan (2009)

[25]. A. E. Lutz; R. J. Kee; J. F. Grcar; F. M. Rupley, *"OPPDIF: A Fortran program for computing opposed-flow diffusion flames"*. Sandia National Laboratories Report SAND96-8243 (1996)

[26]. R. J. Kee; F. M. Rupley; E. Meeks; J. A. Miller, *"CHEMKIN-III: A FORTRAN chemical kinetics package for the analysis of gas-phase chemical and plasma kinetics"*. Sandia National Laboratories Report SAND96-8216 (1996)

[27]. J. Li; Z. Zhao; A. Kazakov; F. L. Dryer, *"An updated comprehensive kinetic model of hydrogen combustion"*. International Journal of Chemical Kinetics 36 (10) (2004) 566-575

[28]. T. Lu; C. K. Law, *"Toward accommodating realistic fuel chemistry in large-scale computations"*. Progress in Energy and Combustion Science 35 (2) (2009) 192-215

[29]. T. Lu; C. S. Yoo; J. H. Chen; C. K. Law, *"Analysis of a turbulent lifted hydrogen/air jet flame from direct numerical simulation with computational singular perturbation"*. 46th AIAA Aerospace Sciences Meeting and Exhibit, Reno, Nevada (2008)

[30]. C.S. Yoo; E. Richardson; R. Sankaran; J. H. Chen, *"DNS of a Turbulent Lifted Ethylene/Air Jet Flame in an Autoignitive Coflow–Stabilization and Flame Structure"*. 9th Turbulent Non-premixed Flames Workshop Motreal, Canada (2008)

[31]. J. H. Chen; A. Choudhary; B. de Supinski; M. DeVries; E. Hawkes; S. Klasky; W. Liao; K. Ma; J. Mellor-Crummey; N. Podhorszki, *"Terascale direct numerical simulations of turbulent combustion using S3D"*. Computational Science & Discovery 2 (2009) 015001

[32]. T. J. Poinsot; S. Lelef, *"Boundary conditions for direct simulations of compressible viscous flows"*. Journal of Computational Physics 101 (1) (1992) 104-129

[33]. J. C. Sutherland; C. A. Kennedy, *"Improved boundary conditions for viscous, reacting, compressible flows"*. Journal of Computational Physics 191 (2) (2003) 502-524

[34]. C. S. Yoo; H. G. Im, *"Characteristic boundary conditions for simulations of compressible reacting flows with multi-dimensional, viscous and reaction effects"*. Combustion Theory and Modelling 11 (2) (2007) 259-286

[35]. C. S. Yoo; Y. Wang; A. Trouvé; H. G. Im, *"Characteristic boundary conditions for direct simulations of turbulent counterflow flames"*. Combustion Theory and Modelling 9 (4) (2005) 617-646

[36]. R. J. Kee; J. A. Miller; G. H. Evans; G. Dixon-Lewis, *"A computational model of the structure and extinction of strained, opposed flow, premixed methane-air flames"*. Symposium (International) on Combustion 22 (1) (1989) 1479-1494

[37]. M. Nishioka; C. Law; T. Takeno, *"A flame-controlling continuation method for generating S-curve responses with detailed chemistry"*. Combustion and Flame 104 (3) (1996) 328-342

[38]. J. Grcar, *"The Twopnt program for boundary value problems"*. Sandia National Laboratories Report SAND91-8230 (1991)

[39]. M. Frenklach; H. Wang; C. L. Yu; M. Goldenberg; C. T. Bowman; R. K. Hanson; D. F. Davidson; E. J. Chang; G. P. Smith; D. M. Golden; W. C. Gardiner; V. Lissianski, *"An Optimized Detailed Chemical Reaction Mechanism for Methane Combustion"*. http://www.me.berkeley.edu/gri_mech/ (1995)

[40]. T. Lu; C. K. Law, *"A directed relation graph method for mechanism reduction"*. Proceedings of the Combustion Institute 30 (1) (2005) 1333-1341